Geophysical Research Letters

RESEARCH LETTER
10.1029/2018GL079550

Key Points:
- Noise correlations to detect subsurface changes prior to their surface manifestation
- Spatial and temporal eruption precursors of a submarine volcano
- Potential of change point analysis of waveform similarity for real-time volcanic hazard assessment

Supporting Information:
- Supporting InformationS1
- Movie S1

Correspondence to:
P. Sánchez-Pastor,
psanchezsp@gmail.com

Citation:
Sánchez-Pastor, P., Obermann, A., & Schimmel, M. (2018). Detecting and locating precursory signals during the 2011 El Hierro, Canary Islands, submarine eruption. *Geophysical Research Letters*, *45*. https://doi.org/10.1029/2018GL079550

Received 17 JUL 2018
Accepted 13 SEP 2018
Accepted article online 17 SEP 2018

Detecting and Locating Precursory Signals During the 2011 El Hierro, Canary Islands, Submarine Eruption

Pilar Sánchez-Pastor[1], Anne Obermann[2], and Martin Schimmel[1]

[1]Institute of Earth Sciences Jaume Almera-CSIC, Barcelona, Spain, [2]Swiss Seismological Service, ETH Zürich, Zurich, Switzerland

Abstract Forecasting and monitoring submarine volcanic eruptions represent a particular challenge due to the lack of direct surface observations. In the present study, we investigate the dynamics of the 2011 El Hierro submarine eruption using phase autocorrelation and cross-correlation from 2 years of continuous seismic records. Time evolution analysis of the waveform similarity allows us to clearly identify different preeruptive phases of this new volcano, as well as three magmatic intrusions that occurred in 2012. We use probabilistic sensitivity kernels to locate the places of the highest dynamics within the magmatic accumulation zone and the extinct volcanic area of Tiñor that might have acted as stress barriers, guiding the magma from the North of El Hierro Island to the final eruption site at the South. Our results highlight the potential of ambient noise methods to monitor volcanic hazard and unrest even with sparse data sets and limited knowledge of the region.

Plain Language Summary In 2011, a new volcano in the Canary Archipelago emerged at the southern edge of El Hierro Island after the archipelago had shown 40 years of quiescence. The volcanic eruption was submarine and unexpected, which impeded setting up instruments around the volcanic edifice and far in advance. This limited spatial distribution of instruments and the scarce data set of observables represent a particular challenge in forecasting and monitoring submarine volcanoes and motivated our research. We analyze the volcanic activity using 2 years of continuous seismic records from El Hierro Island. Our approaches involve methods from seismic interferometry as autocorrelation and cross correlation to determine waveform changes related to the different phases of volcanic activity and probabilistic sensitivity kernels of wave propagation to locate the places of the highest dynamics within the magmatic accumulation zone. Our results highlight the potential of ambient noise methods to forecast and monitor volcanic hazard and unrest even with sparse data sets in less known regions.

1. Introduction

Accurate volcanic hazard monitoring is an important step to mitigate the associated risk at local and regional scale. Standard equipment to deliver near-real-time observables includes GPS, tiltmeters, gas monitoring, cameras, and seismometers. While most before-mentioned methods are limited to surface observations, the analysis of seismic data provides a look at the processes occurring in the volcano interior. A standard tool is the study of the presence, quantity, and migration of microseismicity, which can yield important information about forthcoming and ongoing eruptions (e.g., Armbruster et al., 2014; Peng & Rubin, 2016; Roman, 2017). In the last decade, the study of waveform changes in the coda of seismic ambient noise correlations emerged as a complementary tool to gain information about ongoing deformations in the subsurface due to the movement of pressurized volcanic fluids that alter the elastic and scattering properties of the surrounding medium (e.g., Brenguier et al., 2008; De Plaen et al., 2016; Obermann, Planès, Larose, & Campillo, 2013). Studying the interior dynamics is of particular importance for submarine volcanoes, where direct surface measurements are not available.

In 2011, a new volcano in the Canary Archipelago emerged at the Southern edge of El Hierro Island after the Canary archipelago had shown 40 years of quiescence. The volcanic eruption was preceded by an intense seismic unrest with a characteristic migration over time from the Northern El Golfo region toward the final eruption site at the southern tip of the island (Figure 1). Over the past years, this eruption has been studied in depth to elucidate the associated processes with different approaches: tomographic studies (García-Yeguas et al., 2014; Martí et al., 2017), modeling of the geodetic pressure sources (López, Benito-Saz, et al., 2017), microseismic sounding methods (Gorbatikov et al., 2013), and fractal dimension analysis (López

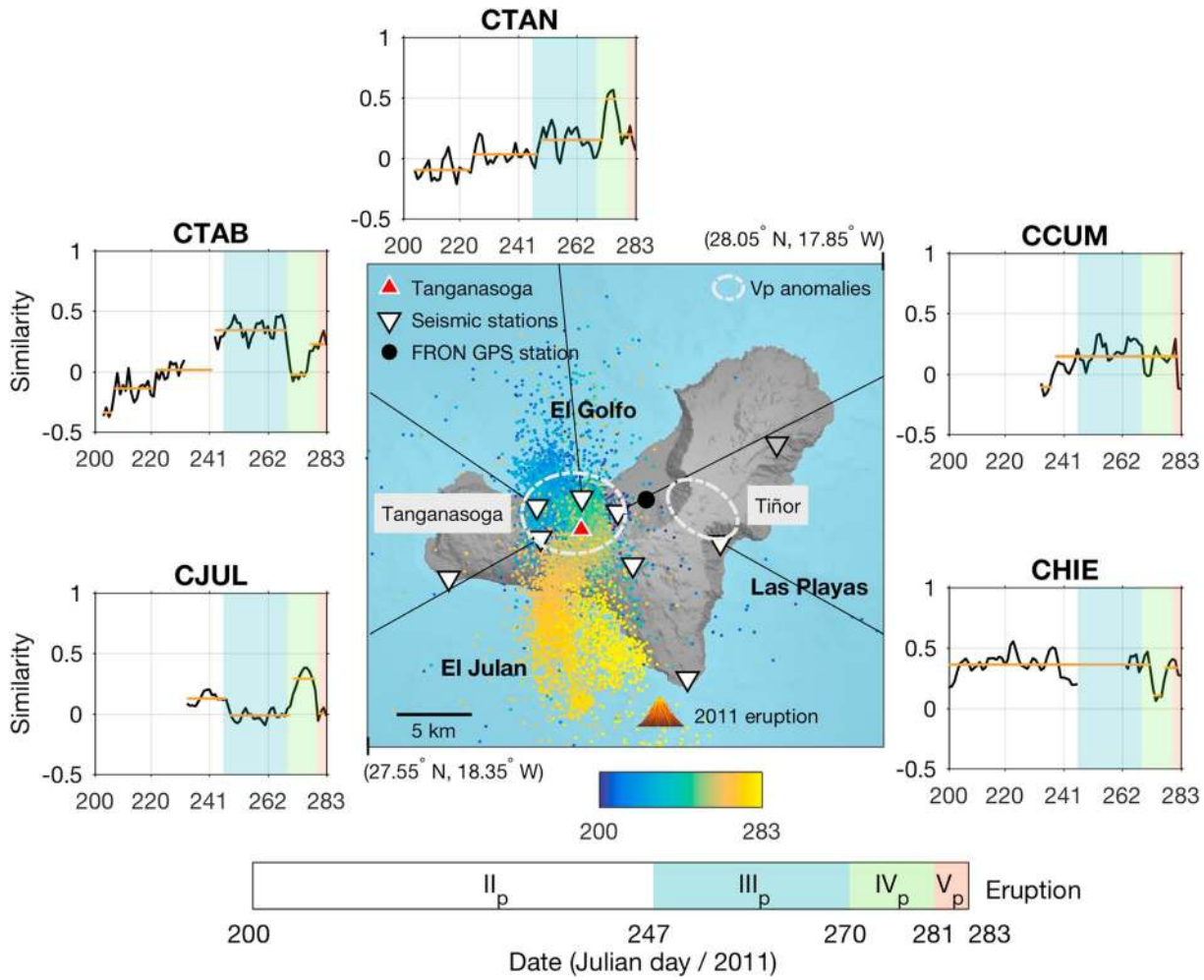

Figure 1. Inner part: Map of El Hierro Island. Inverted triangles mark the location of the seismic stations. The station in gray has been discarded due to problems with its frequency content. The black dot marks the GPS station FRON. The time evolution of the seismicity prior to the eruption in 2011 is marked with colored dots. The gray dashed circles highlight the Tanganasoga and Tiñor volcanic areas that are marked by high V_p anomalies (Martí et al., 2017). Outer part: Similarity curves at 16–22 s of lag time for various autocorrelations. Orange, horizontal lines mark time periods delimited by abrupt changes in the average of the waveform similarity, as obtained from the change point analysis. Background colors indicate the preeruptive phases of López et al. (2012) and are labeled with the subscript *p*.

et al., 2014). Precursory unrest indicators have been suggested from on-land GPS and seismicity data (e.g., López et al., 2012; López, García-Cañada, et al., 2017).

In our study, we investigate the potential of ambient noise correlation combined with coda wave interferometry to shed light on the dynamic evolution of the El Hierro submarine volcano, with a special focus on the preeruptive period in 2011 and three intrusions throughout 2012. Working with a sparse data set, we put emphasis on the accuracy, sensitivity, and statistical relevance of our findings. We use phase autocorrelation (AC) and phase cross correlation (CC, Schimmel, 1999) to increase the temporal accuracy of the correlations and study the time evolution of waveform similarity at various coda lag time windows. The statistically relevant changes of the different phases of the 2011 preeruptive and changes related to the 2012 intrusive periods are mapped in 2-D using probabilistic sensitivity kernels. We then discuss and interpret our results in comparison with other geophysical studies.

2. Framework of the El Hierro Eruption

The new submarine El Hierro volcano is situated on the southern flank of the homonymous island that forms part of the Canary Archipelago (Figure 1) at 900 m below sea level (Martí, Castro, et al., 2013) and about 5-km

distance from the town of La Restinga. The El Hierro Island, with the oldest subaerial rocks of 1.2 Ma, is the youngest island of the volcanically active Canary Archipelago, located at its southwestern corner (Guillou et al., 1996). Over the past few thousand years, the most important eruptions in El Hierro are related to Tanganasoga, a volcano inside the El Golfo depression (Figure 1) and the extinct volcanic area of Tiñor in the east/northeast of the island (Figure 1). Both regions are clearly noticeable as high velocity zones in tomography and microseismic sounding studies that show feeding channels down to 10 km (García-Yeguas et al., 2014; Gorbatikov et al., 2013; Martí et al., 2017). Both studies could also highlight a significant magmatic accumulation at depth below the central part of El Hierro Island.

The Canary archipelago has been volcanically active with several eruptions in the last five centuries (Carracedo, 1994). After the 1971 eruption of Teneguia in La Palma (Martí, Pinel, et al., 2013), the archipelago remained in quiescence for four decades.

In July 2011, a sudden onset of microseismic activity was observed at the north of El Hierro Island in the El Golfo depression (Figure 1, phase II_p). The microseismic activity was produced by a magmatic intrusion that manifested itself in terms of surface deformation (López et al., 2012). More than 11,000 seismic events were detected, migrating southward crossing the island (phase III_p). After a short period of acceleration of the volcanic processes (phase IV_p), the unrest culminated after a few days of system stabilization (phase V_p) in the volcanic eruption of El Hierro submarine volcano. The eruption started on 10 October 2011 on a north-south trending fissure in the southern flank of the island (Martí, Pinel, et al., 2013), with the onset of strong volcanic tremor. However, the first surface observations in terms of strong bubbling due to degassing appeared a few days later (López et al., 2012). For comparison with our results, the phases of unrest as defined in López et al., 2012 are marked in color in Figure 1. The dominant frequency of the tremor oscillates from 0.5 to 1.9 Hz during the eruption period (Tárraga et al., 2014). The tremor lasted until late February 2012 (Figures 2a and 2b), but a clear end of the eruption could not be defined by previous studies. The regional government emergency committee (PEVOLCA) announced the end of the eruption on 5 March 2012. This was the first eruption on the Canary Islands to be monitored in real time by various geophysical instruments from the Spanish National Geographic Institute.

From 2012 to 2014, several magmatic intrusions have been inferred at different parts of the island, which, however, did not culminate in eruptions (Díaz-Moreno et al., 2015; Garcia et al., 2014; González et al., 2013; Klügel et al., 2015; Meletlidis et al., 2015; Telesca et al., 2016).

3. Data and Methods

3.1. Seismic Data and Preprocessing

We analyze 2 years of ambient seismic noise records from seven broadband stations and one short-period station deployed by the Spanish National Geographic Institute in 2011 (white triangles, Figure 1). Two stations covered the beginning of the unrest in July 2011; a total of six stations were running by mid-August, and additional two were set up in October, including the station at the southern tip of El Hierro Island. We compare our results with surface deformation measurements from a GPS station, FRON, belonging to the Canarian Regional Government (black circle, Figure 1). There was an additional seismic station (CTIG, marked in gray in Figure 1), which was located in direct vicinity of a wind park and recorded perturbed waveforms in the frequency bands of interest.

The available data are scarce, and detectable medium changes are likely smaller than observed in volcano monitoring studies, where the stations could be located directly on the volcanic edifice (e.g., Brenguier et al., 2008; Grêt, 2005; Obermann, Planès, Larose, & Campillo, 2013; Takano et al., 2017). Therefore, we use the phase CC (Schimmel, 1999) instead of the classical correlation. Phase CC enables a quicker convergence rate since the data do not require preprocessing to reduce the amplitude bias caused by seismicity and other energetic signals, and it has an intrinsic higher sensitivity to small waveform changes in comparison to the classical correlation (Schimmel et al., 2011, 2018). The approach has been employed successfully in other noise-based monitoring and imaging studies (e.g., D'Hour et al., 2015; Romero & Schimmel, 2018).

As we want to associate observed temporal changes solely to processes in the subsurface, we have to work in frequency bands that are not subject to intense source fluctuations, which likely are not compensated by secondary scattering (Zhan et al., 2013). Different frequency bands have been tested, and the band (2.0–6.0) Hz

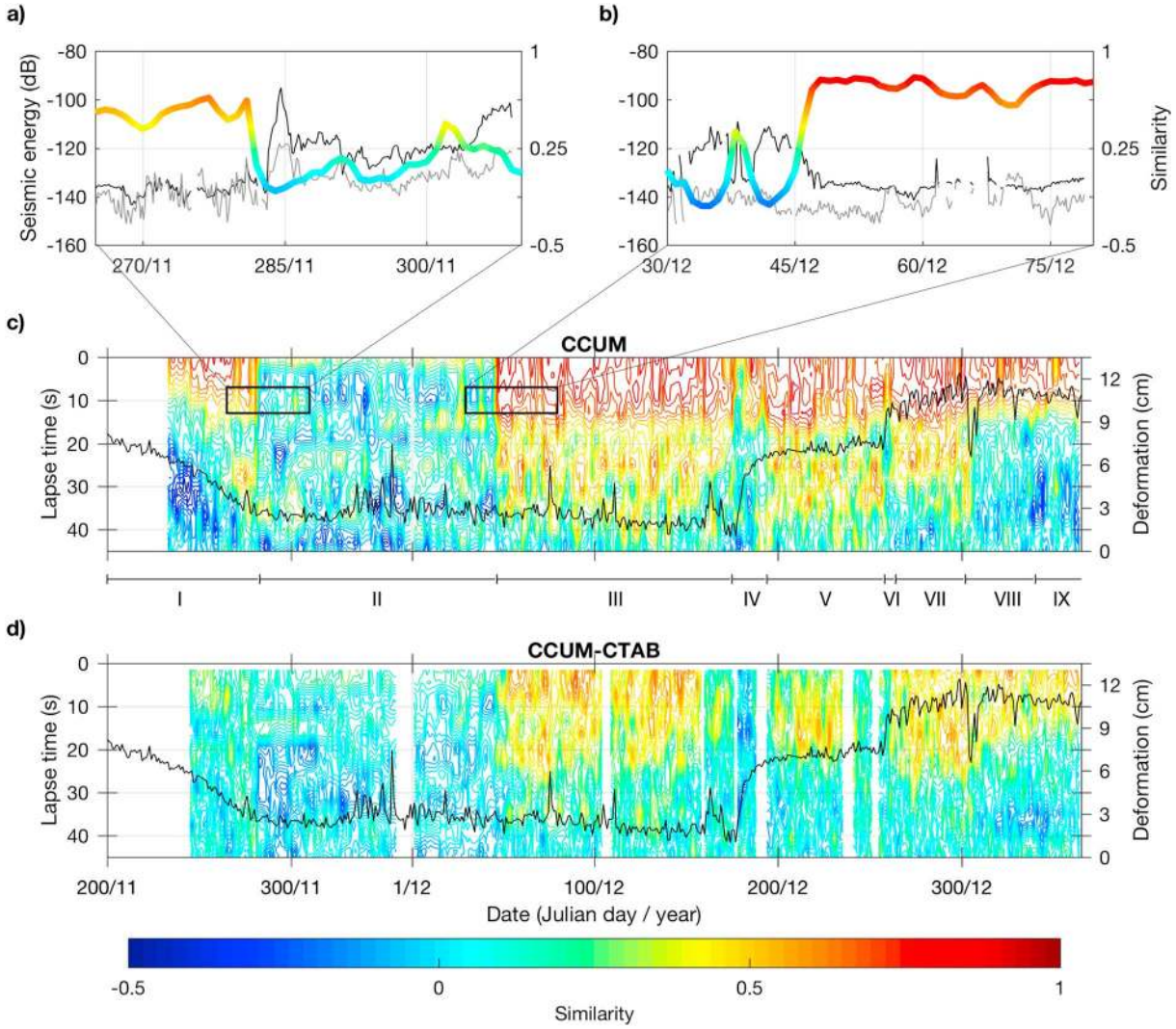

Figure 2. (c, d) Lag time-dependent waveform similarity for the 2 years of study from autocorelation (CCUM) and cross correlation (CCUM-CTAB). The black line represents the modulus of the three components of the surface deformation estimated from GPS station FRON. We mark nine periods of volcanic activity (I–IX). (a, b) Zoom into the waveform similarity around 10-s lag time for the beginning and end of the volcanic eruption. The seismic energy calculated for CCUM is shown at 1 (black) and 4 Hz (gray).

turned out to be optimal, since it provides the most stable seismic response during time intervals without volcanic activity. The chosen frequency band overlaps with the dominant tremor frequencies, which can change the wave field fluctuations significantly. We therefore restrict the study to noneruptive periods.

Our data preparation consists of the following steps: (1) Cutting and decimating the recordings into 1-hr-long segments at 50-Hz sampling frequency, discarding segments with more than 10^4 missing samples. (2) Deconvolving the instrument response function to ground velocity. (3) Applying a 2.0- to 6.0-Hz band-pass filter. (4) Computing ACs and CCs for the vertical component of all station combinations at (−50, 50) seconds lag time. (5) Stacking the correlations linearly with a 3-day sliding data window. This window length is long enough to retrieve stable noise responses during the calm periods.

3.2. Time Evolution of Waveform Similarity

Our main objective is to identify precursory signals and different phases of volcanic activity for the 2 years of interest. We determine the similarity between the daily correlations (CC^{curr}) and their corresponding reference trace (CC^{ref}) as the zero-lag cross correlation in sliding 7-s-long lag time windows with 3-s overlap

within the coda. Thus, we obtain the time dependent waveform similarity as a function of the lag time window j and day of measurement i as

$$S_{ij} = PCC\left[CC_j^{\text{ref}}, CC_{ij}^{\text{curr}}\right]$$

CC^{ref} is calculated stacking all correlations excluding the eruption period (283/2011 to 50/2012). We average negative and positive lag time similarity values.

In Figures 2c and 2d we show the waveform similarity of a typical AC and CC with the respective reference trace at various lag times until the end of 2012. The similarity ranges from -1 (anticorrelation, blue) to 1 (identical, red). Similarity, values are higher for ACs than CCs (Figures 2c and 2d).

Throughout the 1.5 years, we can identify various patterns, which are distinguished by marked similarity changes (I–IX, Figure 2). The low similarity values (period II) correspond to the eruption with intense tremor activity. The waveform similarity allows to clearly identify the beginning (283/2011) and ending (46/2012) of the eruption (Figures 2a and 2b). We here plot the mean of the similarity around 10-s lag time (colored lines) together with the daily mean seismic energy at 1 (black) and 4 Hz (gray). One hertz is the dominant tremor frequency (Tárraga et al., 2014), and 4 Hz is the middle of the frequency band we use in this study. While the beginning of the eruption (Figure 2a) was accompanied by strong volcanic tremor and can also be distinguished through the increase of seismic energy, the end of the eruption cannot be clearly determined from the seismic energy (Figure 2b). Throughout period II, the influence of the volcanic tremor is still present in our frequency band of interest and does not allow measuring any structural change during this period.

Additionally, we compare the lag time-dependent similarity with the surface deformation (Figures 2c and 2d) measured at a nearby GPS station (black circle, Figure 1). Sudden rises of surface deformation correlate well with a decrease in similarity over a broad range of lag times (periods IV and VI). Seismic stations with sufficient preeruptive data show a subtler but significant similarity variation prior to eruption, which correlates with a small surface deformation rise within the period I (day 270/2011).

To assess the robustness of our results despite the choice of reference, five other reference traces have been tested (Figure S1 in the supporting information). The choice of reference has an influence on the absolute similarity values but does not change the main pattern.

3.3. Statistical Relevance of Changes in the Preeruptive Phases

To show the statistical relevance of the changes in similarity that we interpret as precursory signals, we use a statistical method to detect potential change points in our data (Killick et al., 2012).

The precursory signals should be related to the magma feeding, which is expected to happen at around 10 km depth, the dominant depth of the seismicity previous to the eruption (López et al., 2012). Considering an empirical apparent velocity for scattered waves of 1 km/s (Gorbatikov et al., 2013; Meier et al., 2010; Zhan et al., 2013), we analyze the similarity changes for autocorrelations in 16- to 22-s lag time windows, to be sensitive to the target depth.

For the statistical analysis, we determine the mean and standard deviation of the waveform similarity during the calm period in the above-mentioned lag time window (period III Figures 2c and 2d).

Minimizing a cost function (Killick et al., 2012), we determine the change points whether the mean of similarity changes significantly. The significance is defined as 1.5 times the characteristic standard deviation during the calm period. In Figure 1, we mark the time periods with statistically different similarity averages with horizontal lines.

We observe clear similarity changes corresponding to the eruptive phases as defined by López et al. (2012; marked with colors in Figure 1 and discussed in section 2). The advantage of the change point analysis is that it offers an automatic tool to discriminate periods without significant changes in the studied variable.

3.4. Two-Dimensional Spatial Distribution of Structural Changes

To locate medium changes, we use a linear least squares inversion procedure (Tarantola & Valette, 1982) based on probabilistic sensitivity kernels (e.g., Larose et al., 2010; Obermann, Planès, Larose, Sens-Schönfelder, et al., 2013; Pacheco & Snieder, 2005; Planès et al., 2014; Rosetto et al., 2011). These kernels

describe the intensity of wave propagation with the two-dimensional radiative transfer theory, valid since surface waves are dominant (Paasschens, 1997; Sato, 1993; Shang & Gao, 1988) and can be seen as a probabilistic spatial distribution of the locations of the medium changes. What we invert is the decorrelation that we calculate as the absolute difference between the similarity curves from ACs and CCs at specific time windows, and the average from the calmest period (III). The inversion then provides 2-D scattering cross-section density maps that represent a proxy of the capacity of the medium perturbation to deviate waves that depends on the size and strength of the structural changes. For the construction of the sensitivity kernels, we use a rough approximation of the transport mean free path of 30 km, comparing with attenuation studies of other volcanoes (Del Pezzo et al., 2001; Obermann, Planès, Larose, & Campillo, 2013; Prudencio et al., 2013). Obermann, Planès, Larose, and Campillo (2013) have shown that in this type of inversion, an inaccurate transport mean free path has an influence on the size of the affected area, but not on the horizontal localization itself. At different lag times, the sampled region in the subsurface changes, as the diffusive halo of the coda waves changes. We then consider lag times from 5 to 45 s and sliding lag time windows of 10-s lengths with 50% overlap. In the supporting information (Figure S2) we show that our results barely depend on these approximated parameters.

In Figure 3, we show the scattering cross-section density maps at various lag times for the preeruptive phase (IV_p) in 2011 (a), as well as preintrusion (III, b) and intrusion phases in June 2012 (IV, c), September 2012 (V, d and VI, e), and January 2013 (IX, g). Figure 3f shows a quiet period (III) with absence of any changes. We hence conclude that the inversion does not generate significant medium changes nor artifacts, which might cause ambiguities in the interpretations.

In Figure 3a, we see that the changes due to the 2011 preeruptive phase are located in the interior of the Golfo Valley around the Tanganasoga volcano and toward the east in the extinct volcanic area Tiñor. These areas correspond to regions with strong V_p anomalies at shallow depth (Figure 3a, first panel; Martí et al., 2017). Also, the intrusions in 2012 produce subsurface perturbations in these regions with varying sizes and intensities. The location of the changes during the preintrusion phases, lasting for 20 days in June and 15 days in September 2012 (Figures 3b and 3d) correspond to the location of the final intrusions (Figures 3c and 3e) with lower intensity. For each of the dynamic phases, we added the recorded seismicity during the respective phases. Please note, that the location of seismicity does not correspond to the highlighted areas in the scattering cross-section maps.

To test the robustness of our results, we calculated the inversion systematically removing every single station at 20 s of lag time for the phase IV_p (Figure S3). Given the sparse network, the dependency on the seismic network geometry is evident. Nevertheless, the spatial distribution of the changes persists.

4. Interpretation and Discussion

In the following, we discuss our results in the context of the evolution and dynamics of this new submarine volcano.

The waveform similarity analysis allows us to detect with great detail all five preeruptive phases (Figure 1, outer part) as defined in López et al., 2012 with various methods (GPS, seismicity, gas detection, etc.). Only one station reliably recorded the beginning of the unrest (phase I_p). The second preeruptive phase (II_p) is characterized by an important increase of the seismicity, recording up to 450 events per day. We observe a change in similarity in the middle of II_p by the stations in the North (Figure 1, CTAB and CTAN) that could suggest an additional preeruptive phase, for instance, in the form of strong upwelling of the magma. López, Benito-Saz, et al. (2017) also observe a perturbation in the real-time seismic amplitude measurement for this period but leave the underlying processes uncommented.

The third phase (III_p) is characterized by a southward migration of seismicity. This migration starts after a significant change in the scattering cross section below the Tanganasoga volcano, in fact, the largest change in the cross section that we observe in our study (Movie S1). On day 270 (IV_p beginning) the released seismic energy increased drastically as well as alterations of surface deformation and gas emissions (López et al., 2012). All of our stations detect a strong change in similarity (Figure 1) that starts 2 days prior to the strong surface deformations measured by GPS (Figure 2c, I, 25- to 30-s lag time). We think that we already measure a subsurface imprint of the magma movement that causes the surface deformation. During phase V_p (Figure 1)

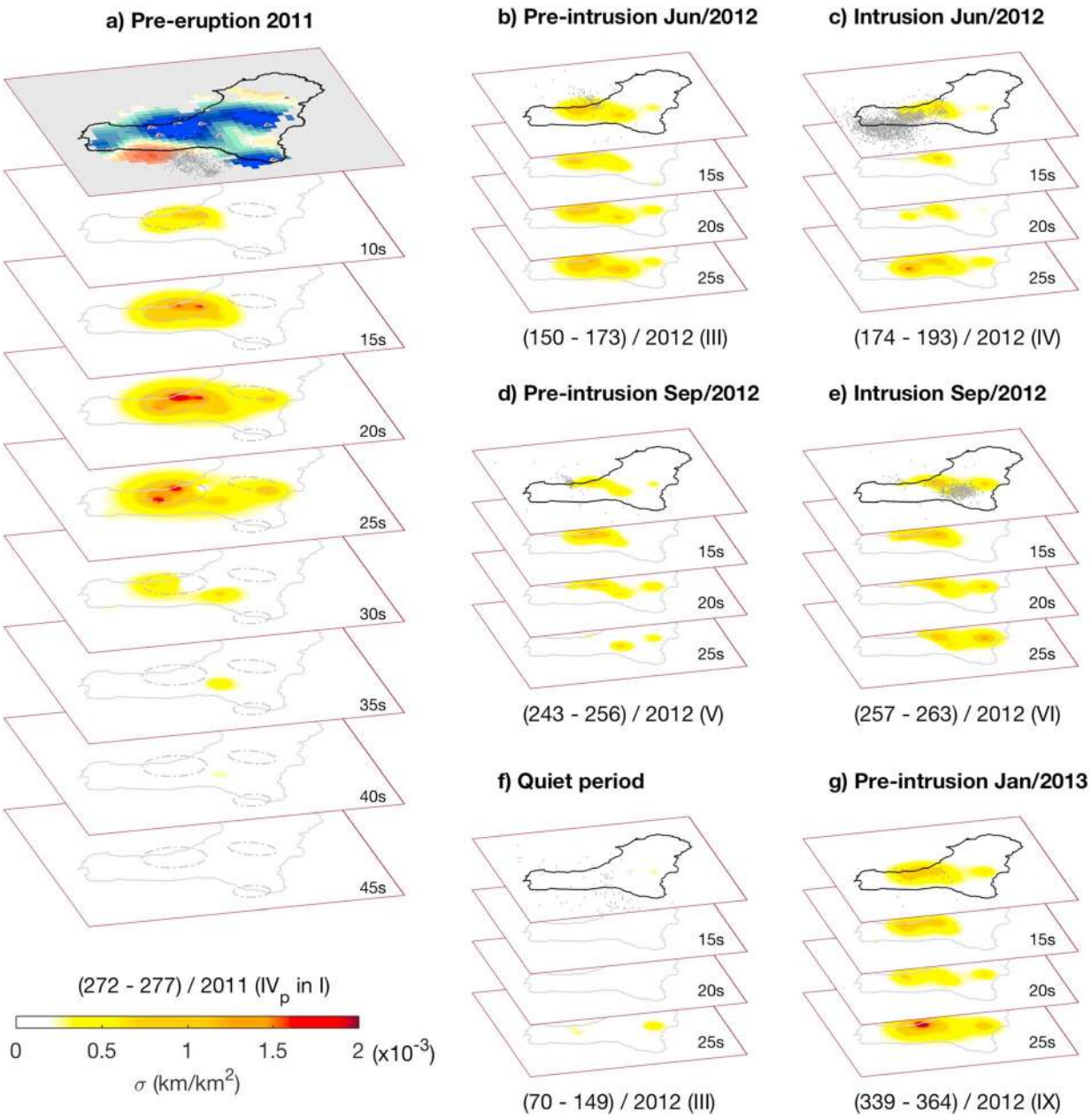

Figure 3. Scattering cross-section density maps at various lag times for different periods. (a) Prior to the eruption. (b, c) Premagmatic and comagmatic intrusion of June 2012. (d, e) Premagmatic and comagmatic intrusion of September 2012. (f) Calmest period. (g) Preintrusion of January 2013. The days averaged are indicated below every panel together with their corresponding time period. The seismicity of the corresponding time periods is marked by gray dots. First panel in (a) represent a *P* wave tomography at 4- to 5-km depth (adapted from Martí et al., 2017). The gray dashed circles in subsequent panels highlight the regions with 8% of V_p perturbations.

prior to the eruption, we observe a short recovery of the similarity values. Such a phase of system stabilization is often preceding volcanic eruptions by days or weeks (e.g., McNutt, 1996).

The El Hierro volcanic eruption initiates the period II (283/2011). This period is clearly identified through a sudden decrease in the measured similarity (Figures 2a, 2c, and 2d). While the beginning of the eruption can also be clearly identified via the volcanic tremor onset (Figure 2a), its end was a question of interpretation (5 March according to PEVOLCA), as the tremor energy decreases erratically (Figure 2b). Here the results from our waveform similarity can clearly set the end of the main magmatic emission to the 15 February (46/2012), where we observe an abrupt increase in similarity. After this day, few lava balloons were observed in the

ocean (Longpre et al., 2014; Martí, Castro, et al., 2013) coinciding in time with some of the observed medium perturbations (Movie S1).

Throughout the year 2012, there were three magmatic intrusions (Figures 2c and 2d, phases IV, VI, and late IX) that, however, did not lead to magmatic eruptions (e.g., Benito-Saz et al., 2017; Lamolda et al., 2017). All three intrusions can be clearly seen in terms of surface deformation on the GPS measurements (Figures 2c and 2d). Coinciding with each change in deformation, we observe a decorrelation of the waveforms (negative or no similarity) that is observed over various lag times (Figures 2c and 2d). When studying the spatial distribution of these changes, the scattering cross-section maps (Figure 3 and Movie S1) show clear precursory perturbations at the location of the final intrusion. The precursory signals typically appear several days prior to the intrusions. The order of magnitude of the scattering cross-section density values are consistent with similar analysis in different environments (Obermann, Planès, Larose, & Campillo, 2013; Obermann et al., 2014).

On the GPS data, we see a very prominent peak on day 302, which seems to be an artifact caused by atmospherics instabilities (Spanish Meteorological Agency, http://www.aemet.es) that produce a delay in the GPS signal. This anomalous behavior coincides in time with the beginning of a similarity perturbation of later lag times in the autocorrelations, which extends until late 2012 (periods VIII–IX).

Tomography studies of El Hierro Island point to two intrusive bodies beneath the island (Figure 3a, first panel). One body is located in the North of El Hierro Island, rises from the lithospheric mantle, and reaches the surface below the Tanganasoga volcano, at the interior of El Golfo Valley (Figure 1). The other body is a vertical feeder channel, located in the eastern zone of El Golfo valley, in the extinct volcanic area of Tiñor (Figure 1). These areas correspond well with the locations of the strongest changes in our scattering cross section maps (Figure 3). The concentration of overpressure in these areas could lead to a significant impact of the scattering properties of the subsurface. We think that our observation confirms that these dense magmatic bodies could act as stress barriers, guiding the magma from the Northern El Golfo region to the Southern tip of El Hierro Island, as observed during the seismicity migration (García-Yeguas et al., 2014; Martí et al., 2017). We observe for all intrusive phases, that the locations of the preintrusion (with little to no indicative seismicity; Figure 3) correspond to the location of the final intrusion, highlighting the potential for precursory alarming. Due to the sparse dataset and limited coverage of the island, we could not follow the migration of magma from the North to South for the eruption in 2011. In 2012, varying numbers of the eight stations are running during the time of the intrusions, but in all cases, the network geometry limits our imaging resolution to the central part of El Hierro Island. We present the scattering cross section maps for different lag times (Figure 3) to get an approximate constraint on the depth of the changes (Obermann, Planès, Larose, Sens-Schönfelder, et al., 2013). The changes are most pronounced at about 20- to 25-s lag time and slowly disappear afterward. The affected region should hence be limited to the upper few kilometers.

5. Conclusions

In this study, we analyzed the waveform similarity from the phase correlations of 2 years of ambient seismic noise in El Hierro Island for a wide range of coda lag times. Marked by significant changes in waveform similarity, we can distinguish several phases of preeruptive unrest related to the appearance of the new submarine volcano El Hierro, at the southern tip of the island in October 2011. We used a change point analysis to test the robustness and significance of our measurements.

Our results allow us to pinpoint the beginning and end of the submarine eruption to exact dates (10 October 2011 to 15 February 2012). In particular the end of the eruption remained vague from previous geophysical studies. Throughout 2012, we could detect and locate subsurface changes related to three magmatic intrusions prior to their surface manifestation. The locations of the changes correspond to feeder channels determined by tomographic studies and are interpreted to act as stress barriers for the magmatic movement.

The data set we analyzed is sparse with a limited spatial coverage. However, we are very optimistic that a denser seismic network would allow us to follow magmatic movements in real time and great detail. Combined with a statistical analysis, such as the change point approach, the data analysis could be automated, providing important information for an early hazard assessment.

Acknowledgments
We would like to thank the Spanish National Geographic Institute (IGN), which participated in the monitoring of the 2011 El Hierro eruption and furnished the waveform seismic records used in this study (volcanologia@fomento.es). The earthquake catalog can be requested from their website (http://www.ign.es). The GPS station FRON belongs to the Canarian Regional Government (GRAFCAN) and can be downloaded from http://www.idecanarias.es/resources/GNSS/Resenias/FRON.pdf. Pilar Sánchez-Pastor acknowledges funding from the Spanish Ministry of Economy and Competitiveness (project MISTERIOS, CGL2013-48601-C2-2-R). The work has benefited from discussions within the EU-funded COST action ES1401 TIDES (TIme DEpendent Seismology). We also thank the Editor Rebecca Carey and two anonymous reviewers for comments that helped improve the manuscript.

References

Armbruster, J. G., Kim, W.-Y., & Rubin, A. M. (2014). Accurate tremor locations from coherent *S* and *P* waves. *Journal of Geophysical Research: Solid Earth*, *119*, 5000–5013. https://doi.org/10.1002/2014jb011133

Benito-Saz, M. A., Parks, M. M., Sigmundsson, F., Hooper, A., & García-Cañada, L. (2017). Repeated magmatic intrusions at El Hierro Island following the 2011–2012 submarine eruption. *Journal of Volcanology and Geothermal Research*, *344*, 79–91. https://doi.org/10.1016/j.jvolgeores.2017.01.020

Brenguier, F., Shapiro, N. M., Campillo, M., Ferrazzini, V., Duputel, Z., Coutant, O., & et al. (2008). Towards forecasting volcanic eruptions using seismic noise. *Nature Geoscience*, *1*(2), 126–130. https://doi.org/10.1038/ngeo104

Carracedo, J. C. (1994). The Canary Islands—An example of structural control on the growth of large oceanic-island volcanoes. *Journal of Volcanology and Geothermal Research*, *60*(3-4), 225–241. https://doi.org/10.1016/0377-0273(94)90053-1

De Plaen, R. S. M., Lecocq, T., Caudron, C., Ferrazzini, V., & Francis, O. (2016). Single station monitoring of volcanoes using seismic ambient noise. *Geophysical Research Letters*, *43*, 8511–8518. https://doi.org/10.1002/2016GL070078

Del Pezzo, E., Bianco, F., & Saccorotti, G. (2001). Separation of intrinsic and scattering Q for volcanic tremor: An application to Etna and Masaya Volcanoes. *Geophysical Research Letters*, *28*, 3083–3086. https://doi.org/10.1029/2001GL013372

D'Hour, V., Schimmel, M., Do Nascimento, A. F., Ferreira, J. M., & Lima Neto, H. C. (2015). Detection of subtle hydromechanical medium changes caused by a small-magnitude earthquake swarm in NE Brazil. *Pure and Applied Geophysics*, *173*(4), 1097–1113. https://doi.org/10.1007/s00024-015-1156-0

Díaz-Moreno, A., Ibáñez, J. M., De Angelis, S., García-Yeguas, A., Prudencio, J., Morales, J., et al. (2015). Seismic hydraulic fracture migration originated by successive deep magma pulses: The 2011–2013 seismic series associated to the volcanic activity of El Hierro Island. *Journal of Geophysical Research: Solid Earth*, *120*, 7749–7770. https://doi.org/10.1002/2015JB012249

Garcia, A., Fernandez-Ros, A., Berrocoso, M., Marrero, J. M., Prates, G., De la Cruz-Reyna, S., & et al. (2014). Magma displacements under insular volcanic fields, applications to eruption forecasting: El Hierro, Canary Islands, 2011–2013. *Geophysical Journal International*, *197*(1), 322–334. https://doi.org/10.1093/gji/ggt505

García-Yeguas, A., Ibáñez, J. M., Koulakov, I., Jakovlev, A., Romero-Ruiz, M. C., & Prudencio, J. (2014). Seismic tomography model reveals mantle magma sources of recent volcanic activity at El Hierro Island (Canary Islands, Spain). *Geophysical Journal International*, *199*(3), 1739–1750. https://doi.org/10.1093/gji/ggu339

González, P. J., Samsonov, S. V., Pepe, S., Tiampo, K. F., Tizzani, P., Casu, F., et al. (2013). Magma storage and migration associated with the 2011–2012 El Hierro eruption: Implications for crustal magmatic systems at oceanic island volcanoes. *Journal of Geophysical Research: Solid Earth*, *118*, 4361–4377. https://doi.org/10.1002/jgrb.50289

Gorbatikov, A. V., Montesinos, F. G., Arnoso, J., Stepanova, M. Y., Benavent, M., & Tsukanov, A. A. (2013). New features in the subsurface structure model of El Hierro Island (Canaries) from low-frequency microseismic sounding: An insight into the 2011 Seismo-volcanic crisis. *Surveys in Geophysics*, *34*(4), 463–489. https://doi.org/10.1007/s10712-013-9240-4

Grêt, A. (2005). Monitoring rapid temporal change in a volcano with coda wave interferometry. *Geophysical Research Letters*, *32*, L06304. https://doi.org/10.1029/2004GL021143

Guillou, H., Carracedo, J. C., Perez-Torrado, F. J., & Rodriguez Badiola, E. (1996). K-Ar ages and magnetic stratigraphy of a hotspot-induced, fast grown oceanic island—El Hierro, Canary Islands Author links open overlay panel. *Journal of Volcanology and Geothermal Research*, *73*(1-2), 141–155. https://doi.org/10.1016/0377-0273(96)00021-2

Killick, R., Fearnhead, P., & Eckley, I. A. (2012). Optimal detection of changepoints with a linear computational cost. *Journal of the American Statistical Association*, *107*(500), 1590–1598. https://doi.org/10.1080/01621459.2012.737745

Klügel, A., Longpré, M.-A., García-Cañada, L., & Stix, J. (2015). Deep intrusions, lateral magma transport and related uplift at ocean island volcanoes. *Earth and Planetary Science Letters*, *431*, 140–149. https://doi.org/10.1016/j.epsl.2015.09.031

Lamolda, H., Felpeto, A., & Bethencourt, A. (2017). Time lag between deformation and seismicity along monogenetic volcanic unrest periods: The case of El Hierro Island (Canary Islands). *Geophysical Research Letters*, *44*, 6771–6777. https://doi.org/10.1002/2017gl074494

Larose, E., Planes, T., Rossetto, V., & Margerin, L. (2010). Locating a small change in a multiple scattering environment. *Applied Physics Letters*, *96*(20). https://doi.org/10.1063/1.3431269

Longpre, M. A., Klugel, A., Diehl, A., & Stix, J. (2014). Mixing in mantle magma reservoirs prior to and during the 2011-2012 eruption at El Hierro, Canary Islands. *Geology*, *42*(4), 315–318. https://doi.org/10.1130/g35165.1

López, C., Benito-Saz, M. A., Martí, J., del-Fresno, C., García-Cañada, L., Albert, H., & et al. (2017). Driving magma to the surface: The 2011–2012 El Hierro volcanic eruption. *Geochemistry, Geophysics, Geosystems*, *18*, 3165–3184. https://doi.org/10.1002/2017gc007023

López, C., Blanco, M. J., Abella, R., Brenes, B., Cabrera Rodríguez, V. M., Casas, B., et al. (2012). Monitoring the volcanic unrest of El Hierro (Canary Islands) before the onset of the 2011–2012 submarine eruption. *Geophysical Research Letters*, *39*, L13303. https://doi.org/10.1029/2012GL051846

López, C., García-Cañada, L., Martí, J., & Domínguez Cerdeña, I. (2017). Early signs of geodynamic activity before the 2011–2012 El Hierro eruption. *Journal of Geodynamics*, *104*, 1–14. https://doi.org/10.1016/j.jog.2016.12.005

López, C., Martí, J., Abella, R., & Tarraga, M. (2014). Applying fractal dimensions and energy-budget analysis to characterize fracturing processes during magma migration and eruption: 2011–2012 El Hierro (Canary Islands) submarine eruption. *Surveys in Geophysics*, *35*(4), 1023–1044. https://doi.org/10.1007/s10712-014-9290-2

Martí, J., Castro, A., Rodriguez, C., Costa, F., Carrasquilla, S., Pedreira, R., & et al. (2013). Correlation of magma evolution and geophysical monitoring during the 2011–2012 El Hierro (Canary Islands) submarine eruption. *Journal of Petrology*, *54*(7), 1349–1373. https://doi.org/10.1093/petrology/egt014

Martí, J., Pinel, V., López, C., Geyer, A., Abella, R., Tárraga, M., & et al. (2013). Causes and mechanisms of the 2011–2012 El Hierro (Canary Islands) submarine eruption. *Journal of Geophysical Research: Solid Earth*, *118*, 823–839. https://doi.org/10.1002/jgrb.50087

Martí, J., Villasenor, A., Geyer, A., López, C., & Tryggvason, A. (2017). Stress barriers controlling lateral migration of magma revealed by seismic tomography. *Scientific Reports*, *7*(1), 40757. https://doi.org/10.1038/srep40757

McNutt, S. R. (1996). Seismic monitoring and eruption forecasting of volcanoes: a review of the state-of-the-art and case histories. In *Monitoring and mitigation of volcano hazards* (pp. 99–146). Berlin, Heidelberg: Springer.

Meier, U., Shapiro, N. M., & Brenguier, F. (2010). Detecting seasonal variations in seismic velocities within Los Angeles basin from correlations of ambient seismic noise. *Geophysical Journal International*. https://doi.org/10.1111/j.1365-246X.2010.04550.x

Meletlidis, S., Di Roberto, A., Cerdeña, I. D., Pompilio, M., García-Cañada, L., Bertagnini, A., et al. (2015). New insight into the 2011–2012 unrest and eruption of El Hierro Island (Canary Islands) based on integrated geophysical, geodetical and petrological data. *Annals of Geophysics*, *58*(5), S0546. https://doi.org/10.4401/ag-6754

Obermann, A., Froment, B., Campillo, M., Larose, E., Planès, T., Valette, B., et al. (2014). Seismic noise correlations to image structural and mechanical changes associated with the Mw7.9 2008 Wenchuan earthquake. *Journal of Geophysical Research: Solid Earth*, *119*, 3155–3168. https://doi.org/10.1002/2013JB010932

Obermann, A., Planès, T., Larose, E., & Campillo, M. (2013). Imaging preeruptive and coeruptive structural and mechanical changes of a volcano with ambient seismic noise. *Journal of Geophysical Research: Solid Earth*, *118*, 6285–6294. https://doi.org/10.1002/2013jb010399

Obermann, A., Planès, T., Larose, E., Sens-Schönfelder, C., & Campillo, M. (2013). Depth sensitivity of seismic coda waves to velocity perturbations in an elastic heterogeneous medium. *Geophysical Journal International*, *194*(1), 372–382. https://doi.org/10.1093/gji/ggt043

Paasschens, J. C. J. (1997). Solution of the time-dependent Boltzmann equation. *Physical Review E*, *56*(1), 1135–1141. https://doi.org/10.1103/PhysRevE.56.1135

Pacheco, C., & Snieder, R. (2005). Time-lapse travel time change of multiply scattered acoustic waves. *The Journal of the Acoustical Society of America*, *118*(3), 1300–1310. https://doi.org/10.1121/1.2000827

Peng, Y., & Rubin, A. M. (2016). High-resolution images of tremor migrations beneath the Olympic Peninsula from stacked array of arrays seismic data. *Geochemistry, Geophysics, Geosystems*, *17*, 587–601. https://doi.org/10.1002/2015GC006141

Planès, T., Larose, E., Margerin, L., Rossetto, V., & Sens-Schönfelder, C. (2014). Decorrelation and phase-shift of coda waves induced by local changes: Multiple scattering approach and numerical validation. *Waves in Random and Complex Media*, *24*(2), 99–125. https://doi.org/10.1080/17455030.2014.880821

Prudencio, J., Del Pezzo, E., García-Yeguas, A., & Ibáñez, J. M. (2013). Spatial distribution of intrinsic and scattering seismic attenuation in active volcanic islands, I: Model and the case of Tenerife Island. *Geophysical Journal International*, *195*(3), 1942–1956. https://doi.org/10.1093/gji/ggt361

Roman, D. C. (2017). Automated detection and characterization of harmonic tremor in continuous seismic data. *Geophysical Research Letters*, *44*, 6065–6073. https://doi.org/10.1002/2017gl073715

Romero, P., & Schimmel, M. (2018). Mapping the basement of the Ebro Basin in Spain with seismic ambient noise autocorrelations. *Journal of Geophysical Research: Solid Earth*, *123*, 5052–5067. https://doi.org/10.1029/2018jb015498

Rosetto, V., Margerin, L., Planès, T., & Larose, E. (2011). Locating a weak change using diffuse waves (LOCADIFF): Theoretical approach and inversion procedure. *Journal of Applied Physics*, *109*, 034903. https://doi.org/10.1063/1.3544503

Sato, H. (1993). Energy transportation in one- and two-dimensional scattering media-analytic solutions of the multiple isotropic scattering model. *Geophysical Journal International*, *112*(1), 141–146. https://doi.org/10.1111/j.1365-246X.1993.tb01443.x

Schimmel, M. (1999). Phase cross correlations: Design, comparisons, and applications. *Bulletin of the Seismological Society of America*, *89*(5), 1366–1378.

Schimmel, M., Stutzmann, E., & Gallart, J. (2011). Using instantaneous phase coherence for signal extraction from ambient noise data at a local to a global scale. *Geophysical Journal International*, *184*(1), 494–506. https://doi.org/10.1111/j.1365-246X.2010.04861.x

Schimmel, M., Stutzmann, E., & Ventosa, S. (2018). Low-frequency ambient noise autocorrelations: Waveforms and Normal modes. *Seismological Research Letters*, *89*, 1488–1496. https://doi.org/10.1785/0220180027

Shang, T., & Gao, L. (1988). Transportation theory of multiple scattering and its application to seismic coda waves of impulsive source. *Scientia Sinica*, *31*, 1503–1514.

Takano, T., Nishimura, T., & Nakahara, H. (2017). Seismic velocity changes concentrated at the shallow structure as inferred from correlation analyses of ambient noise during volcano deformation at Izu-Oshima, Japan. *Journal of Geophysical Research: Solid Earth*, *122*, 6721–6736. https://doi.org/10.1002/2017JB014340

Tarantola, A., & Valette, B. (1982). Generalized non-linear inverse problems solved using the least-squares criterion. *Reviews of Geophysics*, *20*(2), 219–232.

Tárraga, M., Martí, J., Abella, R., Carniel, R., & López, C. (2014). Volcanic tremors: Good indicators of change in plumbing systems during volcanic eruptions. *Journal of Volcanology and Geothermal Research*, *273*, 33–40. https://doi.org/10.1016/j.jvolgeores.2014.01.003

Telesca, L., Lovallo, M., López, C., & Marti Molist, J. (2016). Multiparametric statistical investigation of seismicity occurred at El Hierro (Canary Islands) from 2011 to 2014. *Tectonophysics*, *672-673*, 121–128. https://doi.org/10.1016/j.tecto.2016.01.045

Zhan, Z., Tsai, V. C., & Clayton, R. W. (2013). Spurious velocity changes caused by temporal variations in ambient noise frequency content. *Geophysical Journal International*, *194*(3), 1574–1581. https://doi.org/10.1093/gji/ggt170